Journal of Sound and Vibration (1998) **210**(2), 231–241

MODELING OF SILICON WAFER VIBRATION IN SEMICONDUCTOR PROCESS TOOLS

E. R. Marsh, B. J. Maher

Department of Mechanical Engineering, The Pennsylvania State University, University Park, PA 16802, U.S.A.

AND

C. L. White

Equipment Engineering Section, Motorola MOS 12 Die Manufacturing, Communications and Advanced Consumer Technologies Group, Chandler, AZ 85224, U.S.A.

(*Received* 21 *June* 1997, *and in final form* 16 *September* 1997)

An investigation of the behavior of bare, unprocessed silicon wafers during their loading and transport in wafer cassettes is documented. Semiconductor process tools can generate sufficient vibration to cause the current 200-mm diameter wafers to vibrate inside the cassettes leading to particle generation, mechanical misalignment, and wafer walking. The cassettes feature chamfered slots into which the wafers are inserted. In the interest of minimizing particle generation in the cleanroom environment, the wafers slide loosely into the slots. As a result, the wafers show distinct pitching and rattling behavior under certain excitation conditions. A study of the wafer dynamics, when positioned in the cassette slots, shows that the wafers make a transition to instability under repeatable conditions of excitation frequency and amplitude. The development of two models of the wafer behavior is included, as well as an experimental verification of the model's results for 200-mm wafers. The model is expected to predict the behavior of future wafer sizes including the 300-mm wafers now under development.

© 1998 Academic Press Limited

1. INTRODUCTION

Semiconductor process tools are widely acknowledged to occasionally exhibit undesirable vibration levels. Sources include vacuum pumps, actuators, rotating imbalances, and cooling fans. Minimization of particle generation is critical to process yield, so the wafers are transported and stored in plastic cassettes. The cassettes, whose geometry is dictated by industry standards have two vertical columns of 25 chamfered slots on which the wafers rest. The wafers, when placed in the cassette, rest on two points of contact formed by each pair of chamfered slots. The slots provide no constraint in the vertical direction because the slots must be large enough to allow robotic manipulators to insert wafers without abrading the cassette. As a result, the wafers have been shown to walk in the cassette slots and rattle when exposed to process tool vibration. Particle generation, reorientation of the wafers, and catastrophic failure have all been observed depending on the nature of machine excitation.

Figure 1 shows a cassette and a single wafer. The 7.5° chamfer (β) facilitates loading and suppresses wafer vibration in the cross axis (Y) direction. The wafers are particularly sensitive to machine vibration in the vertical (Z) direction.

0022–460X/98/070231 + 11 $25.00/0/sv971329

© 1998 Academic Press Limited

The wafers show two distinct types of undesirable dynamic behavior. At low frequencies, the wafers pitch about the Y-axis as a result of the chamfered slot rails. The resulting oscillation occurs at 8 Hz in 200-mm wafers. At higher frequencies, the modes of vibration of the wafers can be excited. Once excited, the wafers tend to walk or rattle in the cassette. This leads to excessive wafer motion and particle generation. In a matter of minutes or seconds, the wafers can travel the length of the slot and fall out of the cassette.

The wafers, when exposed to excessive base excitation from the semiconductor process tools, lose contact with the chamfered rail slots when the gravity preload is exceeded. For the purposes of discussion, the initial loss of contact will be referred to as the stability threshold. Under high speed video, the wafer can be seen to bounce between the upper and lower rails once the stability threshold is exceeded. In practice, the rattling is frequently accompanied by wafer walking. Walking is most prevalent at the modal frequencies of the wafers; in a 200-mm wafer, the first mode occurs at 51 Hz.

The onset of walking and rattling is highly repeatable, regardless of the orientation of the wafers in the cassettes (each wafer is slightly imbalanced as a result of an orientating notch on the perimeter). This paper documents individual explorations of the threshold in the X, Y, and Z directions revealing the effects that govern wafer stability. The stability limit is conveniently considered as a function of excitation amplitude and frequency [1, 2]. The work also includes the development and experimental verification of models representing the rigid body pitching and bending dynamics.

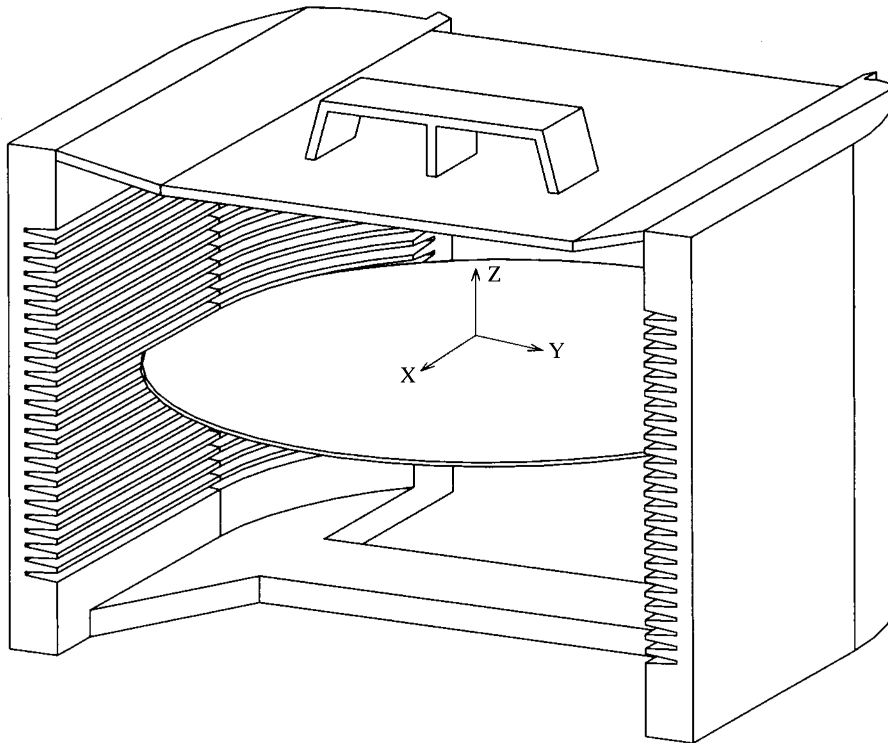

Figure 1. Schematic of a cassette loaded with a single wafer showing orientation of reference frame used throughout this study.

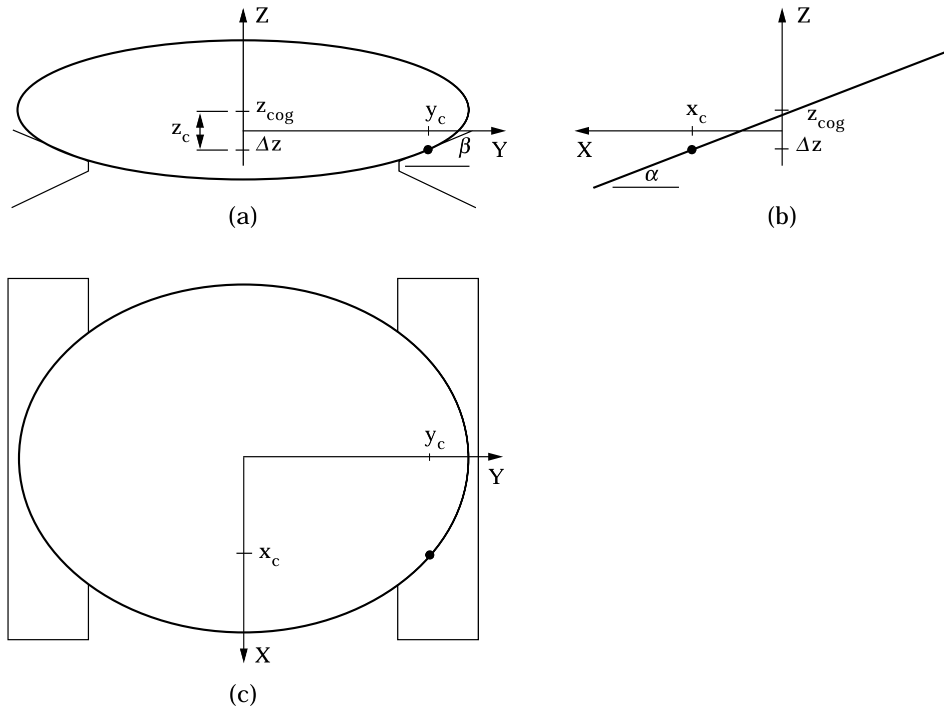

Figure 2. A rigid silicon wafer during pitching: (a) front, (b) side, and (c) top views.

2. WAFER PITCHING ANALYSIS

The wafer pitch model developed in this section predicts the stability limit of the wafer as a function of the excitation frequency and amplitude. The excitation is taken to occur in the vertical direction as a result of process tool vibration. The resulting pitching oscillation is similar to the classic pendulum problem; however, the contact point location changes as a function of pitch angle. The purpose of developing the model is to understand the issues affecting the wafers' tendency to pitch in the cassettes. This understanding can then be used to predict the pitching of other wafer sizes, including the 300-mm wafers now in development by the semiconductor industry.

The chamfered cassette slots provide an interesting geometry problem that must be solved to develop an adequate model of the wafer pitch dynamics. The pitching motion causes translation of the center of mass in the Z direction. This displacement will be shown to go with the square of the pitch angle α. Pitching also results in a change in the contact point location in the X direction. The location of the contact point in the X direction goes linearly with the pitch angle. The wafer is assumed to remain centered in the slot in the Y direction. Furthermore, the translation of the wafer center of gravity in the X direction can be shown to remain small for most pitch angles.

The geometrical analysis begins by considering the wafer, as projected onto the YZ plane (front view of Figure 2). In this plane, the projection of the circular wafer is an ellipse. The YZ co-ordinates of the contact point (y_c and z_c) and the rise in the center of mass (z_{cog}) are developed as a function of the pitch angle of the wafer (α).

First, the equation of the elliptical projection is written as

$$\frac{y^2}{R^2} + \frac{z^2}{R^2 \sin^2 \alpha} = 1. \tag{1}$$

Using equation (1), an expression for z is found. As suggested by Figure 2, the tangent of the ellipse at the contact point coincides with the cassette rail. Therefore, the expression for z, when differentiated with respect to y, is set equal to the slope of the cassette slot angle β. This eliminates the variable z and relates the Y co-ordinate of the contact point y_c to the pitch angle α, slot angle β, and wafer radius R:

$$y_c = \frac{\pm R \tan \beta}{\sqrt{\sin^2 \alpha + \tan^2 \beta}}. \tag{2}$$

Equation (2) is then substituted into equation (1) to obtain the Z co-ordinate of the contact point z_c,

$$z_c = \frac{R \sin^2 \alpha}{\sqrt{\sin^2 \alpha + \tan^2 \beta}}. \tag{3}$$

The line that is formed by the YZ projection of the cassette rail surface is also used to find Δz, the vertical distance from the contact point to the equilibrium position of the wafer. The rise in the center of mass z_{cog} is then obtained as the sum of the contact point z_c and Δz, as suggested by Figure 2(a):

$$\Delta z = -(R - y_c) \tan \beta, \qquad z_{cog} = z_c + \Delta z = R(\sqrt{\sin^2 \alpha + \tan^2 \beta} - \tan \beta). \tag{4, 5}$$

A similar treatment of the XY projection (top view of Figure 2) provides the relationship between the X co-ordinate of the wafer contact point x_c and the wafer's center of mass:

$$x_c = \frac{R \sin \alpha \cos \alpha}{\sqrt{\sin^2 \alpha + \tan^2 \beta}}. \tag{6}$$

The location of the contact point is now specified as a function of the wafer radius R, the slot angle β, and the pitch angle α. As these relationships suggest, the model of the pitch motion will contain non-linear terms. As shown in Figure 2, if $\alpha > 0$, then $x_c > 0$, $y_c > 0$, $z_{cog} > 0$ and $z_c > 0$. Equations (2), (3), (5) and (6) verify this observation. The cassette geometry restricts the pitch angle α to small values, therefore equations (2), (3), (5) and (6) are approximated by considering only the dominant terms:

$$x_c = \frac{R\alpha}{\tan \beta}, \qquad y_c = R, \qquad z_c = \frac{R\alpha^2}{\tan \beta}, \qquad z_{cog} = \frac{R\alpha^2}{2 \tan \beta}. \tag{7}$$

A wafer, when exposed to low-frequency base excitation in the vertical (Z) direction, responds with a pitching motion. The non-linear differential equation governing the pitching motion is obtained by constructing the Lagrangian of the wafer system subject to the geometric relationships of equation (7):

$$2mr(\ddot{w} + 2r\dot{\alpha}^2 + 2r\ddot{\alpha}\alpha)\alpha + J\ddot{\alpha} + 2rmga = 0, \tag{8}$$

where

$$r = R/2 \tan \beta. \tag{9}$$

The base excitation w, the wafer mass m, the mass moment of inertia J, and gravity g, each contributes to the differential equation describing the wafer pitch behavior. However, the bracketed terms in equation (8) are non-linear, and given the assumption of small pitch angles α, this quantity is neglected, as is the position-dependence of the mass moment of inertia. The solution obtained from the remaining linear terms provides close

agreement to the experimentally measured response that is shown in Figure 3, adequately justifying the small angle assumption.

The linear decay envelope of the wafer pitch response suggests that Coulomb damping is the dominant energy dissipation mechanism for all but the smallest angles.

The tendency for the wafer to lose contact with the cassette rails during pitching is assessed using the linearized differential equation obtained from equation (8) [3],

$$J\ddot{\alpha} + 2rmg\alpha = 0. \tag{10}$$

The base excitation w does not appear in the linearized differential equation of the pitch angle α. This suggests, and has been verified experimentally, that the wafer pitching is not influenced by the base excitation. As a result, the pitching motion that occurs at relatively low frequencies does not influence the wafer's tendency to rattle in the plastic cassettes. Experimental measurements support this conclusion; the wafers do not demonstrate a loss of stability in the frequency range near the pitch frequency.

Equation (10) provides the natural frequency of the pitching motion; substitution of the mass moment of inertia J and the expression for r yield a function of the wafer radius R, the slot angle β, and the gravitational constant g:

$$\omega_n = \sqrt{\frac{2rmg}{J}} = \sqrt{\frac{4g}{R\tan\beta}}. \tag{11}$$

The analysis shows that the wafers do not lose contact with the cassettes as a result of the pitching motion, although undesirable particle generation can occur.

3. WAFER BENDING DYNAMICS

For a variety of wafer sizes, the first bending mode is much higher in frequency than the pitching mode. The bending modes play a significant role in the stability threshold of the wafers. Experience shows that the first bending mode is the most likely to participate

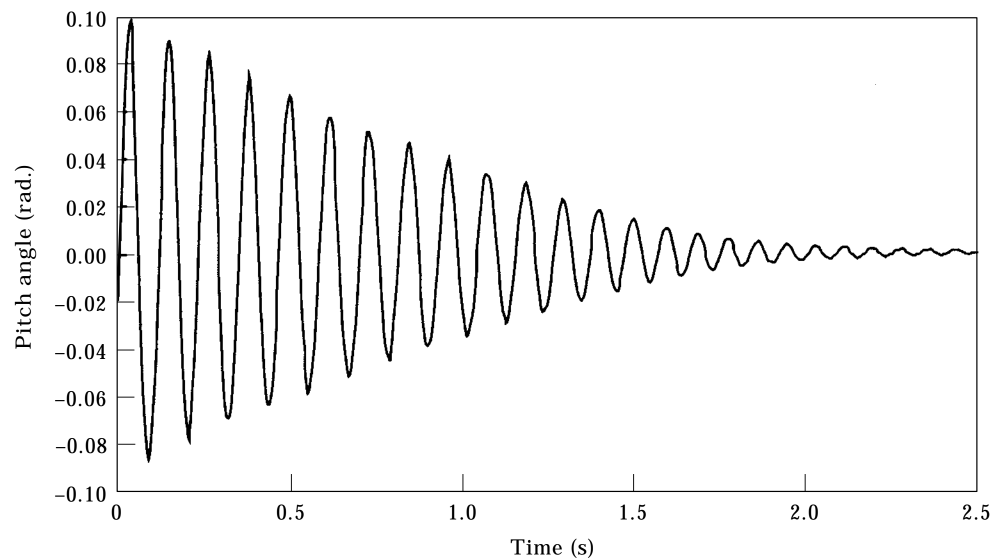

Figure 3. Experimentally measured wafer pitch impulse response.

in rattling, a finding supported by the following analysis. In this section, a general analysis is presented to find the critical base excitation amplitudes that result in wafer instability as a function of frequency.

In the course of this work, a discrepancy was found in published values of Young's modulus of monocrystalline silicon. Therefore, the modulus of production grade silicon wafers is re-evaluated here by measuring the wafers' static deflection with kinematic support under known loads. The calculated value of the Young's modulus of bare, unprocessed monocrystalline silicon is 147 GPa. The density is 2330 kg/m^3, as previously published. These values provide excellent agreement between static and dynamic finite element models and experimental observation.

The analysis proceeds by considering the governing differential equations of motion that dictate the linear dynamics of the wafer bending modes. Symmetry can be invoked to reduce the size of the problem. For example, a single quarter of the wafer can be considered to determine the stability threshold associated with the first mode of vibration.

The contact of the wafer and the cassette slot results in a boundary condition on the corresponding vertical d.o.f. In practice, the exact location of the contact point varies with the pitch angle of the wafer. However, the pitching has been shown to demonstrate negligible coupling with the base excited stability dynamics and is accurately treated separately. To explore the stability limit of the wafer under oscillatory base excitation, a sinusoidal input will be applied to the linear model. The stability limit is then calculated at individual frequencies. First, the ordinary differential equations representing the wafer dynamics are partitioned into block matrices [2, 4],

$$\begin{bmatrix} \mathbf{M}_{11} & \mathbf{M}_{12} \\ \mathbf{M}_{21} & \mathbf{M}_{22} \end{bmatrix} \begin{Bmatrix} \ddot{\mathbf{x}}_1 \\ \ddot{\mathbf{x}}_2 \end{Bmatrix} + \begin{bmatrix} \mathbf{K}_{11} & \mathbf{K}_{12} \\ \mathbf{K}_{21} & \mathbf{K}_{22} \end{bmatrix} \begin{Bmatrix} \mathbf{x}_1 \\ \mathbf{x}_2 \end{Bmatrix} = \begin{Bmatrix} \mathbf{g}_1 \\ \mathbf{g}_2 \end{Bmatrix} + \begin{Bmatrix} \mathbf{N} \\ \mathbf{0} \end{Bmatrix}, \tag{12}$$

where $\mathbf{M}_{11}$ is the mass block matrix of contact point d.o.f. $(q \times q)$, $\mathbf{M}_{22}$ is the mass block matrix of remaining d.o.f. $(p - q \times p - q)$, $\mathbf{K}_{11}$ is the stiffness block matrix of contact point d.o.f. $(q \times q)$, $\mathbf{K}_{22}$ is the stiffness block matrix of remaining d.o.f. $(p - q \times p - q)$, $\mathbf{g}_1$ is the gravity force acting on contact d.o.f. $(q \times 1)$, $\mathbf{g}_2$ is the gravity force on remaining d.o.f. $(p - q \times 1)$, and $\mathbf{N}$ is the reaction force on contact point d.o.f. $(q \times 1)$.

The subscript 1 denotes the d.o.f. associated with the wafer/cassette contact points. In the case of a quarter wafer model, only one contact point is explicitly included and the matrix dimension $q = 3$ (x, y and z d.o.f.). The subscript 2 denotes the remaining d.o.f. in the structural model. The total model dimension is p. The displacement of the d.o.f. associated with the contact point(s) is dictated by the sinusoidal base excitation to the wafer ($\mathbf{x}_1$). The allowable amplitude of the input, $\mathbf{X}_1$, prior to the loss of contact will be determined by setting the contact point reaction force $\mathbf{N} = 0$:

$$\mathbf{x}_1 = \mathbf{X}_1 \sin \omega t. \tag{13}$$

The resulting reponse to the sinusoidal excitation, as well as the static deflection due to the gravity body force, can be written in terms of an unknown static and sinusoidal displacement,

$$\mathbf{x}_2 = \mathbf{A} + \mathbf{X}_2 \sin \omega t. \tag{14}$$

The functions for $\mathbf{x}_1$ and $\mathbf{x}_2$, when substituted into the block matrices of equation (12), yield new equations for the unknowns $\mathbf{A}$, $\mathbf{X}_1$ and $\mathbf{X}_2$. By matching terms, $\mathbf{A}$ and $\mathbf{X}_2$ are

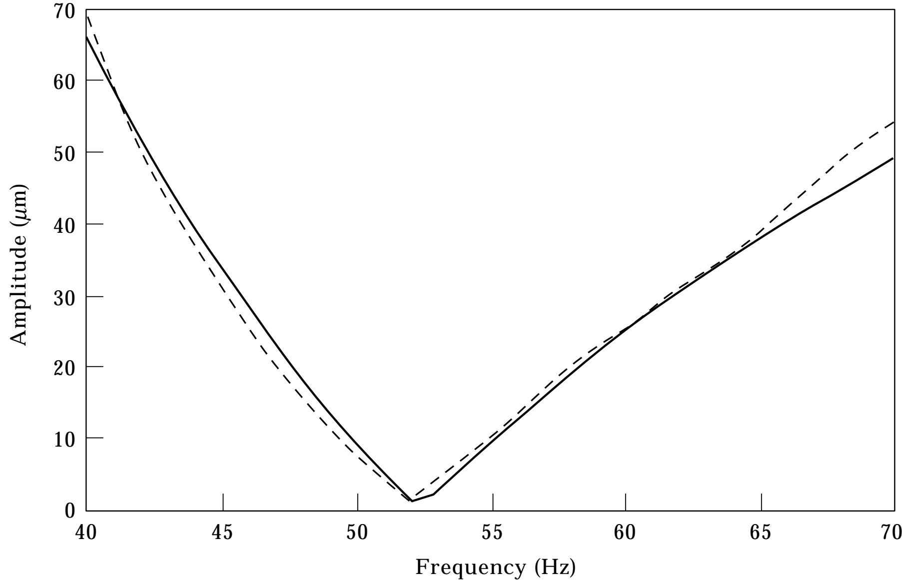

Figure 4. 200-mm wafer stability as a function of frequency: – – –, experimental; ——, analytical.

eliminated to yield an equation relating the input vibration amplitude to the reaction force at the contact point:

$$(\mathbf{Z}_{11} - \mathbf{Z}_{12}\mathbf{Z}_{22}^{-1}\mathbf{Z}_{21})\mathbf{X}_1 \sin \omega t + (\mathbf{K}_{12}\mathbf{K}_{22}^{-1}\mathbf{g}_2 - \mathbf{g}_1) = \mathbf{N}. \tag{15}$$

It can be seen that the wafer will lose contact with the cassette slot when the normal force $\mathbf{N}$ becomes negative. The stability threshold is therefore at $\mathbf{N} = 0$. Because the sinusoidal component of the normal force undergoes a sign change in every cycle of vibration, the wafer first becomes unstable when

$$\mathbf{X}_1 = \left|(\mathbf{Z}_{11} - \mathbf{Z}_{12}\mathbf{Z}_{22}^{-1}\mathbf{Z}_{21})^{-1}(\mathbf{K}_{12}\mathbf{K}_{22}^{-1}\mathbf{g}_2 - \mathbf{g}_1)\right|. \tag{16}$$

Finally, the response of the remaining d.o.f. can be calculated from equation (16) and the original matrix representation of equation (12):

$$\mathbf{X}_2 = -\mathbf{Z}_{22}^{-1}\mathbf{Z}_{21}\mathbf{X}_1, \qquad \mathbf{A} = \mathbf{K}_{22}^{-1}\mathbf{g}_2. \tag{17}$$

This solution, when evaluated numerically for silicon wafers of different sizes, provides the condition under which the wafers may be expected to lose contact with a vibrating surface. In the following section, the solution is verified experimentally.

4. EXPERIMENTAL VERIFICATION OF WAFER STABILITY

The numerical solution of the wfer stability threshold may be evaluated by considering a finite element discretization of the wafer. For this verification, the dynamics of a 200-mm silicon wafer are modelled in quadratic plate elements. The converged mesh is condensed to the vertical d.o.f. using Guyan (static) reduction. The resulting mass and stiffness matrices are used to construct a proportional damping matrix based on the Rayleigh model and a modal damping factor of $\zeta = 0{\cdot}003$. The three matrices are then used to construct the inpedance matrices of equations (16) and (17).

Using equation (16), the stability threshold of a 200-mm wafer is plotted as a function of frequency in Figure 4. Also plotted are experimentally measured stability results.

Experimental verification of the analytical model requires a single-degree-of-freedom flexure allowing motion in the vertical direction. The flexure, which features high stiffness in the off-axis directions, has no modal frequencies in the wafer test range of 0–80 Hz. The semiconductor process tool vibrations that lead to wafer instability are simulated by a Ling electrodynamic shaker driving the flexure and measured using three Kistler accelerometers. A non-contacting Lion precision capacitance probe captures the wafer response.

The stability threshold is determined experimentally by using increasingly large excitation amplitudes at individual test frequencies. At a given frequency, the excitation amplitude is slowly increased until the wafer loses contact with the cassette. The loss of contact is characterized by rattling or X direction wafer motion in the cassette, as measured by the capacitance probe. The wafer stability shows a high degree of repeatability and the threshold is unaffected by location of the wafers in the cassette and wafer orientation.

At frequencies other than the modal bending frequencies, the wafers exhibit a high degree of stability. However, at the first modal frequency (51 Hz for a 200-mm wafer) the stability limit is low (0·61 μm). The drop in stability at resonance is dictated by the amount of damping in the vibration mode (typical measured damping factors vary between 0·0025 and 0·0035). Further exploration of the effect of damping is made by incorporating a suitable damping matrix into the stability model.

Figure 5 plots the stability threshold for three values of damping factor ζ. As expected, the modal damping dictates the response at resonance.

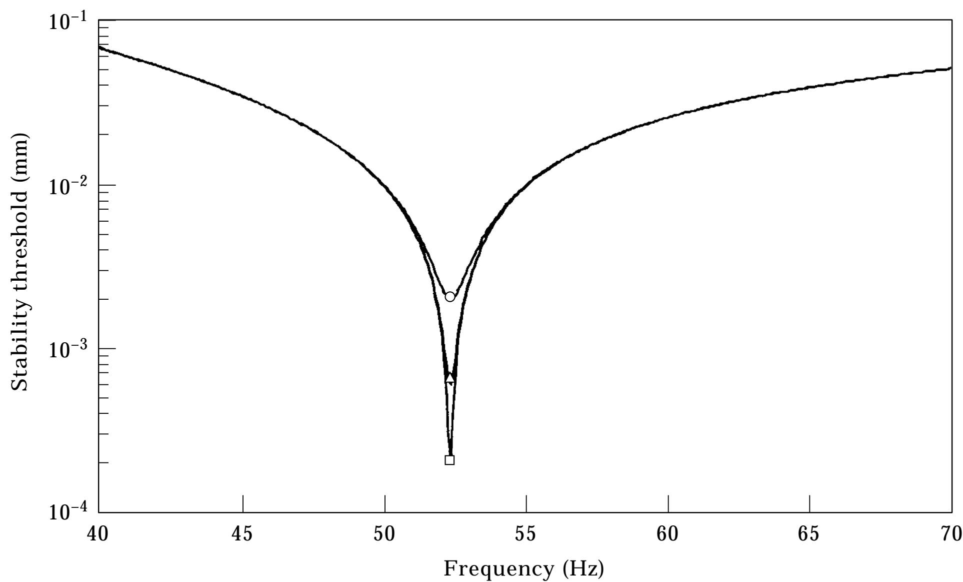

Figure 5. Stability threshold of 200-mm wafer as a function of frequency and three different damping factors: ○, $\zeta = 0{\cdot}010$; △, $\zeta = 0{\cdot}003$, and □, $\zeta = 0{\cdot}001$.

TABLE 1

First mode bending frequencies and stability thresholds of common wafers sizes

Wafer diameter (mm)	Wafer thickness (mm)	First mode bending frequency (Hz)	Critical stability amplitude (μm)
125	0·625	115	0·093
150	0·675	87	0·19
200	0·724	51	0·61
300	0·775	25	3·1

5. USE OF A STABILITY MODEL TO PREDICT BEHAVIOR OF 300-MM WAFERS

As the semiconductor industry turns toward the usage of 300-mm wafers, the sensitivity of larger wafers to vibration becomes an increasingly important issue. To this end, the experimentally verified model is used to determine the stability of other wafer sizes. Smaller wafer sizes that are still in common production are also investigated here for comparison. Table 1 shows the first mode bending frequencies of several common wafer sizes. The critical machine vibration amplitudes that result in instability, as determined using the stability model, are also listed. Figure 6 shows the stability threshold, as a function of machine excitation frequency. The first mode damping factor ζ is taken to be 0·003 for all wafer sizes. The figure shows that the different wafer sizes display similar stability envelopes that differ principally in their modal frequencies. At base excitation acceleration levels above the gravitational constant g, the wafers may be assumed to always be unstable, regardless of frequency.

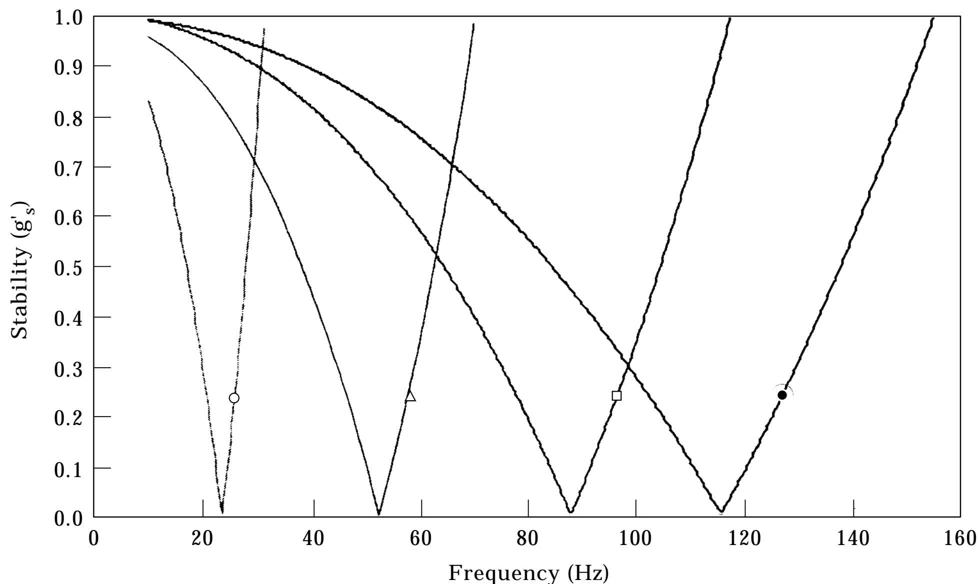

Figure 6. Stability threshold (*g*) of silicon wafers: ○, 125-mm diameter; △, 150-mm diameter; □, 200-mm diameter; and ●, 300-mm diameter.

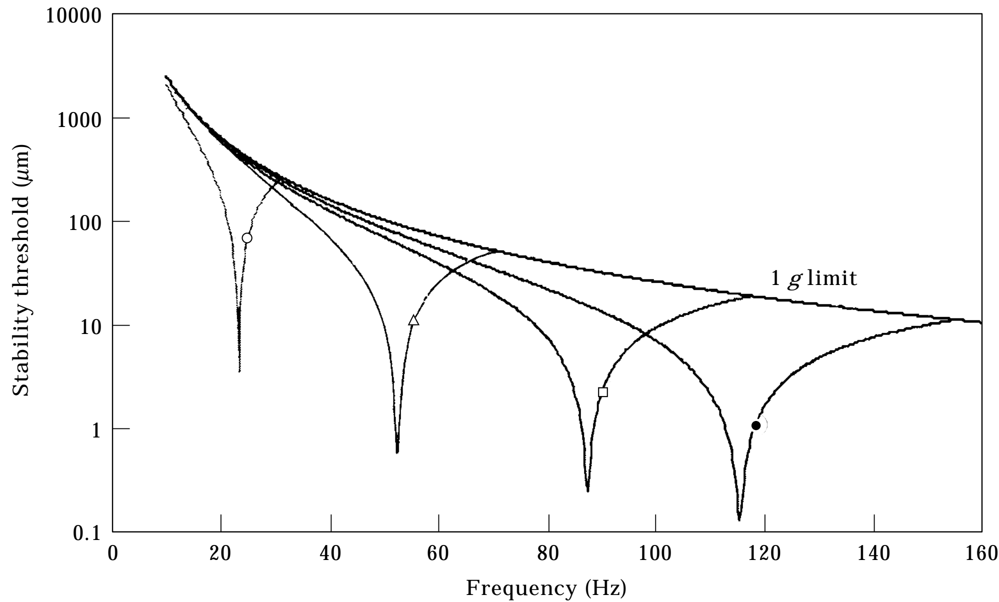

Figure 7. Stability threshold (μm) of silicon wafers: ○, 125-mm diameter; △, 150-mm diameter; □, 200-mm diameter; and ●, 300-mm diameter.

Figure 7 shows the stability threshold of different wafer sizes plotted in terms of base excitation displacement. The 1 g limit is also indicated.

6. CONCLUSION

Two models describing the dynamic behavior of silicon wafers have been developed and verified experimentally. The first model captures the low frequency pitching of the wafers in the slotted cassettes. The results suggest that although the motion may reach significant amplitude, it does not lead to a loss of stability in the wafer. The second model treats the flexible modes of the wafer and their effect on the stability of the wafer. It is shown that these modes greatly reduce the stability of the wafer when exposed to base excitation.

The models allow comparison of the tendency of different wafer sizes to lose contact with the cassettes. Any loss of contact is undesirable because particle generation and wafer breakage may occur. The second stability model suggests that the wafer's resistance to vibration may be improved by an increase of damping. Additional work with the model may lead to modified edge constraints to better support the wafers for dynamic stability.

ACKNOWLEDGMENT

The authors wish to recognize the Motorola Eureka Fund for its generous support of this work.

REFERENCES

1. M. A. DAVIES 1994 *Chaos*, *Solitons and Fractals* **4–2**, 275–283. Transition from soliton to chaotic motion during impact of a nonlinear elastic structure.
2. A. H. NAYFEH 1995 *Applied Nonlinear Dynamics*: *Analytical*, *Computational*, *and Experimental Methods*. New York: Wiley.
3. S. H. CRANDALL 1968 *Dynamics of Mechanical and Electromechanical Systems*. New York: McGraw-Hill.
4. R. R. CRAIG 1981 *Structural Dynamics*, *an Introduction to Computer Methods*. New York: Wiley.
5. L. MEIROVITCH 1967 *Analytical Methods in Vibrations*. New York: Macmillan.

APPENDIX: NOMENCLATURE

J	mass moment of inertia
$\mathbf{K}$	stiffness matrix
$\mathbf{M}$	mass matrix
$\mathbf{N}$	reaction force vector
R	wafer radius
X	x direction in reference frame
Y	y direction in reference frame
Z	z direction in reference frame
g	gravitational constant (9·81 m/s^2)
m	mass
w	base excitation
x_c	location of contact point x direction
y_c	location of contact point in y direction
z_c	location of contact point in z direction
z_{cog}	location of center of mass in z direction
$\mathbf{g}$	gravitational body force vector
$\mathbf{x}$	displacement vector
α	pitch angle
β	slot angle
ω	base excitation frequency
ζ	modal damping factor